Spatiotemporal chaos and nonequilibrium transitions in a model excitable medium

Ashwin Pande and Rahul Pandit*
Centre for Condensed Matter Theory, Department of Physics, Indian Institute of Science, Bangalore 560 012, India

We present a detailed study of the statistical steady states of a model for CO oxidation on Pt(110) proposed by Bär and co-workers. We show that the stability diagram of this model depends sensitively on the boundary conditions. We elucidate several novel properties of a state with meandering spirals (M) briefly mentioned by Bär and co-workers. (1) We show that, with periodic boundary conditions, M is the state MP, a binary mixture displaying a coexistence of quasiperiodically rotating spirals and chaotically moving pointlike defects. We show that the transition from MP to the turbulent state T1 is continuous; the transition line marks the locus where the two phases cease to be distinct. (2) With Neumann boundary conditions M is the state MN, a single quasiperiodically rotating spiral. We show that the MN-T1 transition is discontinuous or first order. We also characterize the transitions from MP and MN to the state S, which has quasiperiodically rotating spirals. We also propose qualitative mechanisms for these transitions.

I. INTRODUCTION

Spiral waves are ubiquitous in two-dimensional excitable media: they occur in a wide variety of systems including some chemical reactions [1], calcium waves in the cell cytoplasm [2], and cardiac arrhythmias [3]. Thus an elucidation of the phenomena exhibited by them is of considerable importance. A particularly interesting class of such phenomena are the transitions from states with steadily rotating spirals to ones with meandering spirals [4] and, sometimes, to those with spatiotemporal chaos. A few groups [1,5,6] have begun to study these transitions in experimental and model systems. We extend these studies by a detailed analysis of one such sequence of transitions in a model proposed in Ref. [1] to describe the oxidation of CO on Pt(110). The possibility of carrying out careful experiments on this system makes this model especially appealing. As a parameter ε (see below) is varied, this model shows a sequence of transitions from a state with steadily rotating spirals (S), to one with meandering spirals (M), and then to turbulent states (T1 and T2) in which there is steady creation and annihilation of spirals. Thus it is well suited for a systematic study of these transitions.

Before proceeding further it is useful to define the model of Ref. [1] for CO oxidation. It consists of the following two coupled partial differential equations in two spatial dimensions $\mathbf{x}$:

$$\frac{\partial u}{\partial t} = \nabla^2 u - \frac{1}{\varepsilon} u(u-1)[u-(v+b)/a], \qquad (1)$$

$$\frac{\partial v}{\partial t} = f(u) - v.$$

Here the fields u and v are related to CO and O coverages [1], a, b, and ε are control parameters related to rate constants, etc., for the chemical reactions involved, t denotes time, and $f(u)=0$ if $u<\frac{1}{3}$, $f(u)=1-6.75u(u-1)^2$ if $\frac{1}{3} \leqslant u<1$, and $f(u)=1$ if $u \geqslant 1$. We use dimensionless variables that are related to those describing CO oxidation on Pt(110) in Ref. [7]. The numerical studies of Ref. [1] have yielded a stability diagram for the statistical steady states of Eq. (1) in the b-ε plane with $a=0.84$: As ε is increased from 0, say with $b=0.07$, a transition occurs from a state S, comprising rigidly rotating spirals, to another state M with meandering spirals; on further increasing ε, M evolves into states T1 and T2 that exhibit spiral turbulence [1]. Other recent studies [6,8] have tried to characterize the chaos that obtains in the states M, T1, and T2. In this paper we present an extensive numerical study of model (1) that focuses on elucidating the natures of the states S, M, T1, and T2 and the transitions between them.

Our principal qualitative results are summarized below: The nature of the state M and, therefore, the transitions from it to the states T1 and S depend sensitively on both (a) the initial conditions and (b) the boundary conditions. The initial-condition dependence has been noted in Ref. [6]; here we restrict ourselves to initial conditions that yield spirals in the statistical steady state and concentrate on the boundary-condition dependence. We study both periodic boundary conditions (PBC's) and Neumann , i.e., no-flux, boundary conditions (NBC's); these yield distinct meandering states, which we denote MP and MN, respectively. The state MN comprises one large meandering spiral [Fig. 1(a)]. The state MP consists of large meandering spirals coexisting with a finite concentration of point defects [Fig. 1(b)]; such coexistence has been noted in Ref. [1]. In MN the largest Lyapunov exponent $\lambda_m \simeq 0$ so this state is barely chaotic; indeed, we suggest below that it is quasiperiodic. MP is chaotic since $\lambda_m > 0$ for it. The MN-T1 transition is first order, e.g., the defect number density jumps discontinuously here [Fig. 2(a)] if ε is moved sufficiently slowly through

*Also at Jawaharlal Nehru Center for Advanced Scientific Research, Bangalore, India.

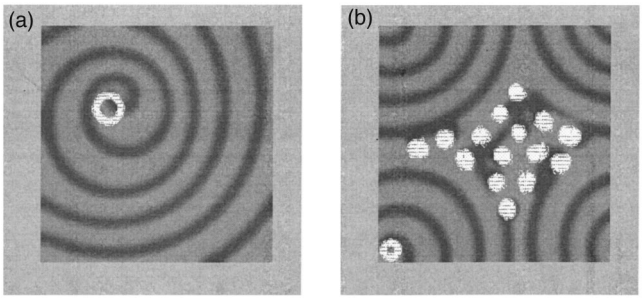

FIG. 1. Gray-scale plots of the u field in (a) the single-spiral state MN and (b) the inhomogeneous state MP at $\varepsilon = 1/15.9 \simeq 0.0629$. The gray intensity is proportional to the field amplitude at that point. The trajectories of the spiral cores or small-defect cores are shown superposed in white. Note the clear ''phase separation'' in the state MP.

$\varepsilon \simeq 0.057$; a hysteresis loop [Fig. 2(b)] is obtained if ε is changed rapidly enough that metastable states do not decay.

By contrast the MP-T1 transition is continuous. The transition can be characterized by the order parameter $S(\mathbf{k}) = 1/4\pi^2 \langle |\int d^2\mathbf{x} e^{i\mathbf{k}\cdot\mathbf{x}} u(\mathbf{x},t)|^2 \rangle$; in a state containing large spirals, $S(\mathbf{k})$ displays a secondary peak at $|\mathbf{k}| = k_c$, where k_c is the wavelength of the spiral arm. If we define $a_{kc} \equiv 1/2\pi \int_{-\pi}^{\pi} d\theta S(k_c \cos(\theta), k_c \sin(\theta))$, we find that a_{kc} rises continuously from 0 as the system moves from the state T1 to the state MP [9].

The MP-S transition is also continuous; in particular, λ_m and the standard deviation σ of the interspike intervals (see below) go to zero as powers of $(\varepsilon - \varepsilon_c)$, where ε_c is the critical value at which the state S appears.

The remaining part of this paper is organized as follows. In Sec. II we describe the numerical methods we use and the quantities we measure in our study of model (1). Section III contains a discussion of our results for the states S, MP, MN, T1, and T2 and the transitions between them. Section IV contains concluding remarks.

II. NUMERICAL STUDIES

To our knowledge, we have carried out the most extensive numerical study of model (1) to date. Our numerical scheme is described below. In this section we define the quantities we have calculated via our numerical solution of this model. The study of Ref. [6] demonstrates that long transients of spatially and temporally irregular behavior occur in model (1) in the parameter ranges corresponding to the states T1 and T2 for systems with linear system size $L > 25$ and run times $t \simeq 1000$; Ref. [6] provides evidence for a divergence of the transient time with increasing L. We have studied the system principally at $L = 64$ and have not seen the breakdown of these states for times as long as 5×10^5 time units (for comparision, the rotation time of one spiral is $\sim 4-5$ time units). On the time scale of our studies the system displays well-defined, nonequilibrium, statistical steady states.

We study Eq. (1) numerically by discretizing it using the method of lines on an evenly spaced square grid of side L, with $2L$ grid points per side, and the standard six-point

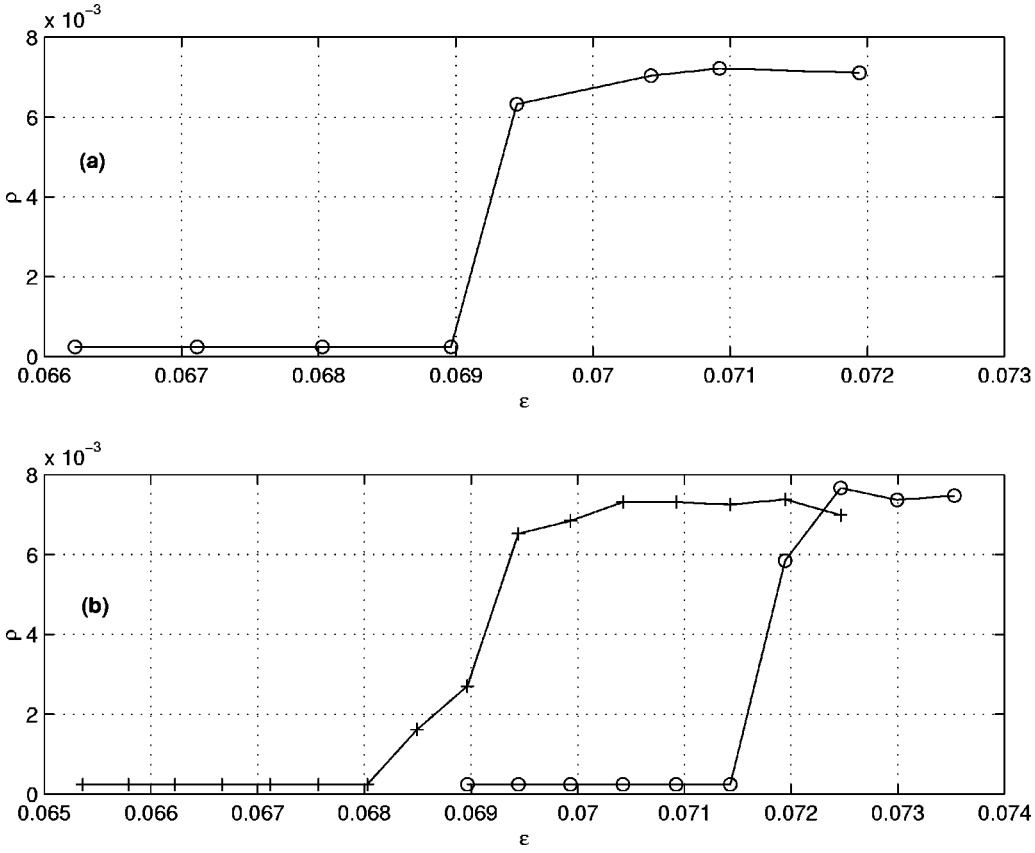

FIG. 2. Plots of (a) ρ vs ε at the MN-T1 transition and (b) the hysteresis loop obtained on varying ε across the transition at a finite rate (see text); o and $+$ indicate decreasing and increasing ε, respectively.

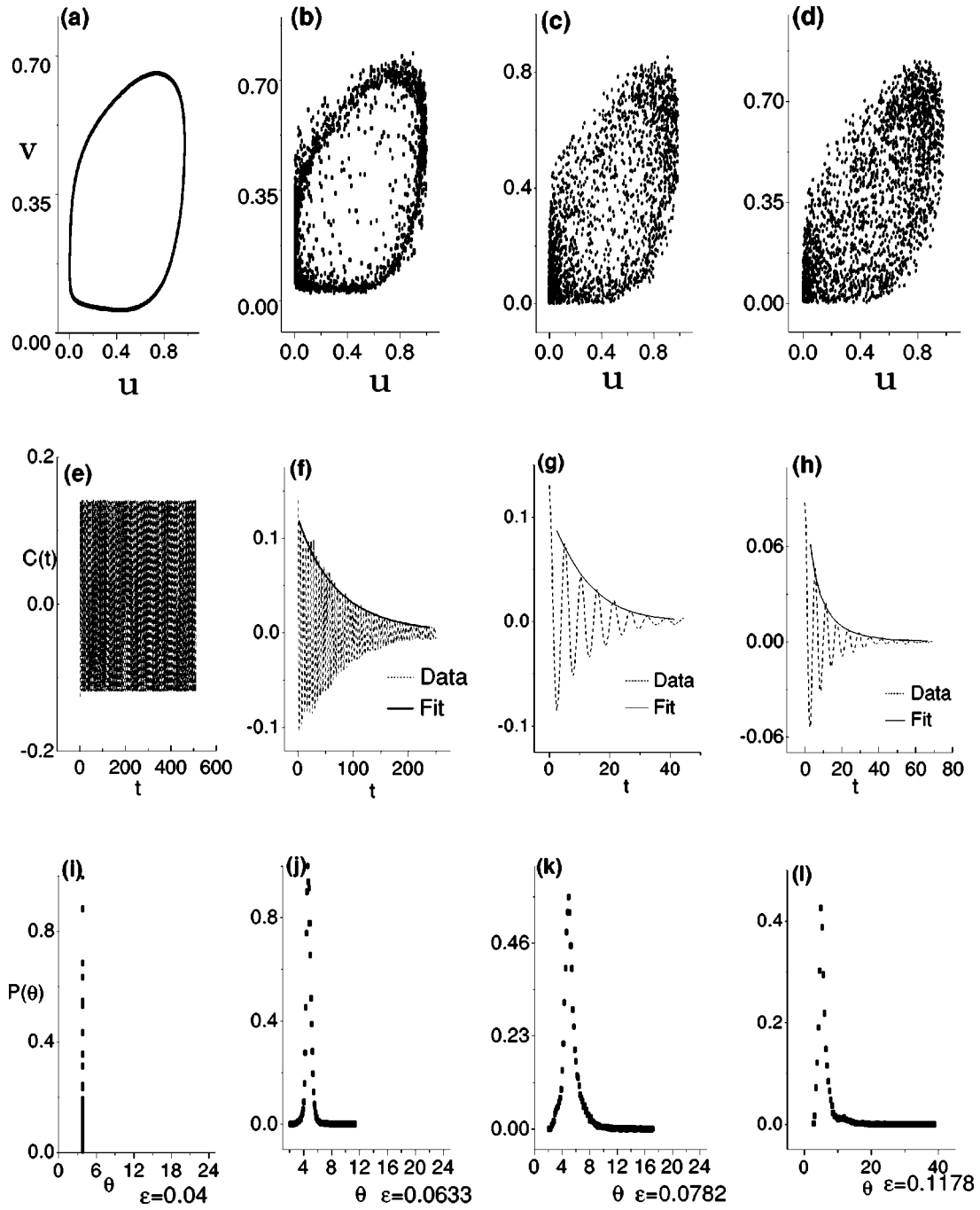

FIG. 3. Local phase portraits with 1000 points each (a)–(d), the temporal autocorrelation function $C(t)$ (e)–(h) (averaged over ten representative grid points), and the distribution $P(\theta)$ (averaged over ten representative grid points) of the interpulse intervals θ in the regimes S ($\varepsilon=0.04$), MP ($\varepsilon=0.0633$), T1 ($\varepsilon=0.0782$), and T2 ($\varepsilon=0.1178$), respectively.

finite-difference stencil for the Laplacian [14]. We normally use $L=64$, but we have checked in representative cases that our results are not modified if $L=128$. We set $a=0.84$, $b=0.07$, and vary ε.

We use both PBC and NBC and, in each case, integrate the resulting system of coupled ordinary differential equations by using a fourth–fifth-order Runge-Kutta scheme with the Cash-Karp parameters and variable step size [14], which suffices for these stiff equations. For very long runs we have used a method proposed by Barkley [5] for integrating these equations; we have checked that both these numerical schemes give consistent results. Our runs with the Barkley integrator are the largest that we know of that have been carried out for model (1) so far.

Local phase portraits, which are plots in the u-v plane of $(u(\mathbf{x},t_n),v(\mathbf{x},t_n))$ for fixed spatial coordinate $\mathbf{x}$ and regularly spaced times t_n, provide a convenient qualitative way to decide whether a state displays simple or complex temporal evolution. For example, with PBC, Figs. 3(a)–3(d) show such phase portraits as ε goes from $0.04-0.1178$, i.e., the system goes from the state S to MP, T1, and then T2: clearly the evolution in S is periodic and increasingly irregular in MP, T1, and T2. We have already noted that MP is inhomogeneous so local phase portraits depend on whether the spa-

tial point $\mathbf{x}$ lies in the region dominated by a large spiral or the region in which clusters of small defects are present. We show representative local phase portraits [Figs. 4(a)–4(b] that illustrate this for the well-separated state of Fig. 1(b). We will show below that the local phase portrait [Fig. 4(a)] obtained from the region of the large spiral corresponds to quasiperiodic and not chaotic behavior. States of the type shown in Fig. 1(b) evolve on very slow time scales ($\sim 10^4$ time units) since the large spirals drift [10].

We calculate autocorrelation functions such as $C(t) \equiv \langle u(\mathbf{x},t_0)u(\mathbf{x},t_0+t)\rangle$ by computing $u(\mathbf{x},t_0)u(\mathbf{x},t_0+t)$ for a range of time lags t and then averaging over sucessive origins of time t_0. These oscillate without decaying in S, but have more and more rapidly decaying envelopes in T1 and T2 [Figs. 3(e)–3(h) for PBC], which can be fit to the form e^{-ct}. A stretched exponential form $\exp(-ct^{\gamma})$, $\gamma<1$, obtains in the state MP if one averages naively over the spatial origin $\mathbf{x}$. However, a more careful average, which accounts for the inhomogeneous nature of MP [see Fig. 1(b)], shows that $C(t)$ has an envelope that hardly decays [Fig. 4(c)] if data are obtained from a point that lies in the region that is dominated by a large spiral; otherwise the envelope of $C(t)$ decays so slowly [Fig. 4(d)] that it can be fitted either to the form $\ln(t)$ or to t^{γ} with $\gamma \simeq 0$ given the precision of our data.

Not surprisingly, then, the envelope of $C(t)$ hardly decays in state MN, which contains one large spiral. Since $\lambda_m > 0$ in state MP but $\lambda_m \simeq 0$ in state MN (see below), we can associate the presence of chaos with the decay of $C(t)$. Furthermore, because $C(t)$ decays only in the regions of state MP, which contain clusters of small defects, we conclude that the chaos arises because of the disorderly motion of these small defects. Given that the envelope of the autocorrelation function $C(t)$ behaves as $\sim\exp(-ct)$ in states T1 and T2, we can extract a correlation time $\tau = c^{-1}$ which decreases as we go from T1 to T2. The variation of this with ε is shown in Fig. 7(d) for PBC. The increase in τ with decreasing ε is clearly visible, again confirming that the phases T1 and T2 display increasingly irregular behavior.

Probability distributions $P(\theta)$ of the time intervals θ between successive pulses in time series of the fast variable u [Figs. 3(i)–3(l), for PBC] are another useful measure of the degree of irregularity of the temporal behavior of the state. Note first that the excitability of the system yields pulses in the time series of $u(\mathbf{x},t)$; representative plots in states S and T2 are shown in Figs. 5(a)–5(b). Given such sequences of pulses, we can obtain the time between successive pulses (or spikes).

This is easier to do in state S, where the spikes are sharp, than in state T2, where they are broader. We define the interspike interval to be the time between two successive crossings of $u(\mathbf{x},t)$ across a threshold u_0 (from below u_0 to above it). We use $u_0 = 0.5$ in most of our studies; however, we have checked that the distributions we get are insensitive to the exact value of u_0 as long as it lies in the middle of the range of values of $u(\mathbf{x},t)$. The probability distribution $P(\theta)$ is a δ function (DF) in state S and broadens in states T1 and T2 [Figs. 3(i)–3(l)]. If one averages naïvely over the spatial origin $\mathbf{x}$ in MP, the resulting PDF is similar to that in T1 [Fig. 3(j)]. However, a more careful average, which accounts for the inhomogeneous nature of MP [see Fig. 1(b)], shows that $P(\theta)$ is nearly bimodal if calculated in the region dominated by a large spiral; otherwise it is broad. Note that $P(\theta)$ in MN yields a similar bimodal distribution, which we associate with the presence of two frequencies in the rotating spiral, namely, the spiral rotation frequency and the meander frequency of the spiral core. We also calculate the standard deviation σ that follows from $P(\theta)$ [Fig. 7(a) for PBC]; it is zero in S and increases in the phases MP, MN, T1, and T2. This confirms that the system displays increasing temporal irregularity in these four phases. However, again we must be careful while calculating σ in the inhomogeneous state MP.

Figure 6(a) shows the temporal power spectrum $S(\omega)$ obtained from the time series of u in MN; Fig. 6(b) is its analog for data obtained from the large-spiral region in MP. In both cases, the peaks in the power spectrum are at sums of integer multiples of two incommensurate frequencies (see Table I).

The ε dependences of the largest Lyapunov exponent λ_m [Figs. 7(b), 7(c) for PBC and Fig. 8(a) for NBC] are also useful in characterizing the evolution from S to MP or MN. We obtain λ_m and the spectrum of Lyapunov exponents by using standard algorithms [11]; we have calculated these spectra only for small system sizes (linear sizes $L=16$ and 32). To obtain reliable estimates for the Lyapunov exponents we follow Ref. [12]: Since the approximation λ_t to a Lyapunov exponent λ is observed to converge as $1/t$, where t is the time over which the integration is done, we estimate λ_m from a fit to the form $\lambda_t = \lambda_m + b/t$. With PBC λ_m is small and negative in S and becomes progressively more positive as we move from MP to T1 and T2; its dependence on boundary conditions is elucidated below. Since calculations of λ_m require knowledge of the time evolution of $u(\mathbf{x},t)$ and $v(\mathbf{x},t)$ for all $\mathbf{x}$, it is not meaningful to try to compute λ_m for separate regions dominated by large spirals or clusters of small defects in MP without making *ad hoc* assumptions. In MP we find that $\lambda_m > 0$.

We define the phase $\phi(\mathbf{x},t) \equiv \tan^{-1}[(v(\mathbf{x},t) - v_*]/[u(\mathbf{x},t) - u_*)]$, with $(u_*, v_*) \simeq (0.66\ldots, 0.484\ldots)$, the unstable fixed point of Eq. (1) without the $\nabla^2 u$ term. This phase winds by 2π around the cores of spiral defects [1] and can be used to obtain the defect density ρ [8,13]. This defect density jumps at the first-order MN-T1 boundary with NBC [Fig. 2(a)] and exhibits hysteretic behavior [Fig. 2(b)] if we cycle through this transition at a finite rate.

The stability diagram of Ref. [1] is valid only for the class of initial conditions that lead to spirals in the statistical steady state that is finally obtained. This is implicit in earlier studies [1] but has not been emphasized sufficiently. We find, e.g., that typical random initial conditions for u and v decay to the uniform state $u=v=0$ at large ε (in MP, MN, T1, and T2). Care must be taken, therefore, to use initial conditions that do yield spirals in the S, MP, MN,T1, and T2 states.

We find that a convenient way of doing this is to start at low ε (deep in state S) with random initial conditions; these usually relax to states with rotating spirals. If we use these relaxed states as initial conditions at larger values of ε, then we obtain a finite number of spiral defects in the steady state. This is true with both PBC and NBC; in the latter case we can also begin with a broken wave front (this eventually curls up into a big spiral).

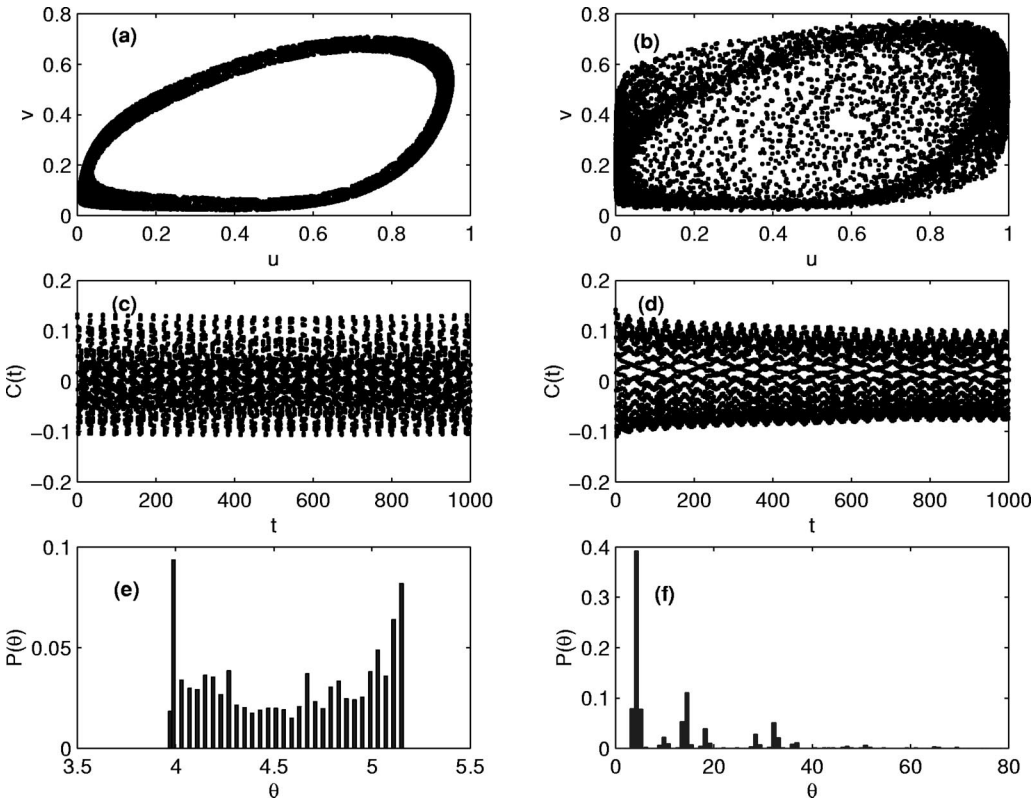

FIG. 4. Plots of (a) the local phase portrait, (c) temporal autocorrelation function $C(t)$, and (e) histogram $P(\theta)$ of the interpulse-intervals θ with data from a large-spiral region in the inhomogenous state MP of Fig. 1(a). Figures (b), (d), and (f) are the analogs of (a), (c), and (e), respectively, with data from the pointlike-defect region of MP for $L=64$.

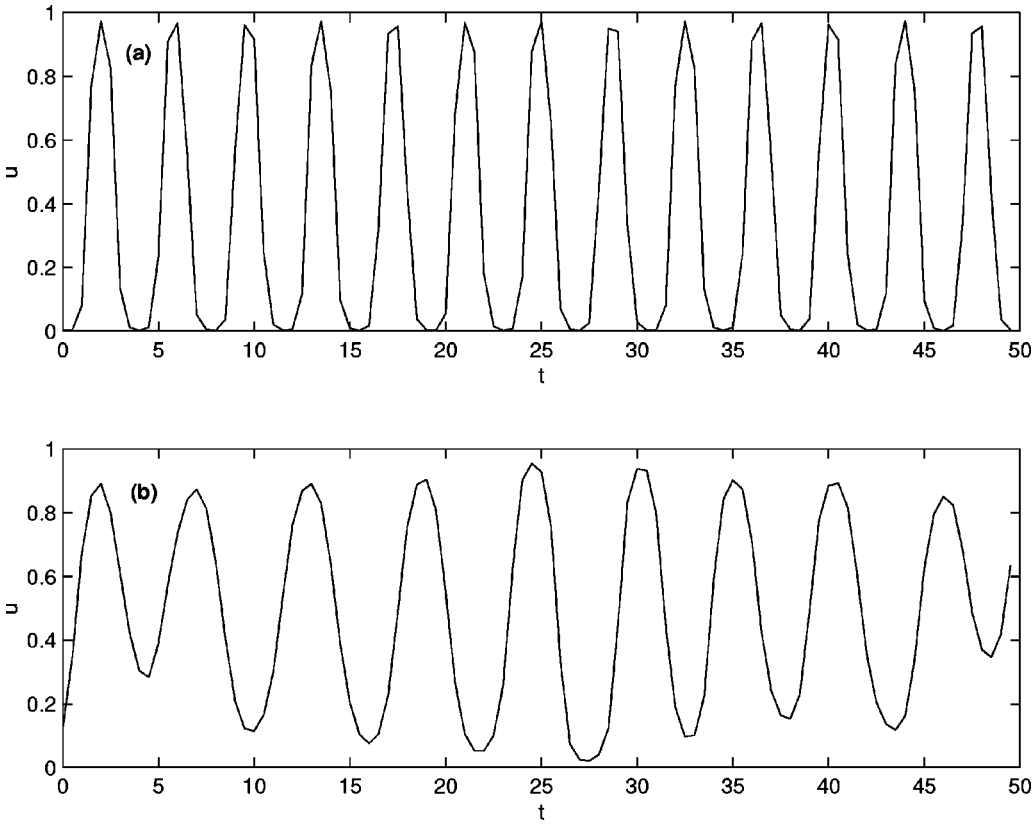

FIG. 5. Plots of $u(\mathbf{x},t)$ vs t for a representative point x in (a) the state S and (b) the state T2 for $L=64$.

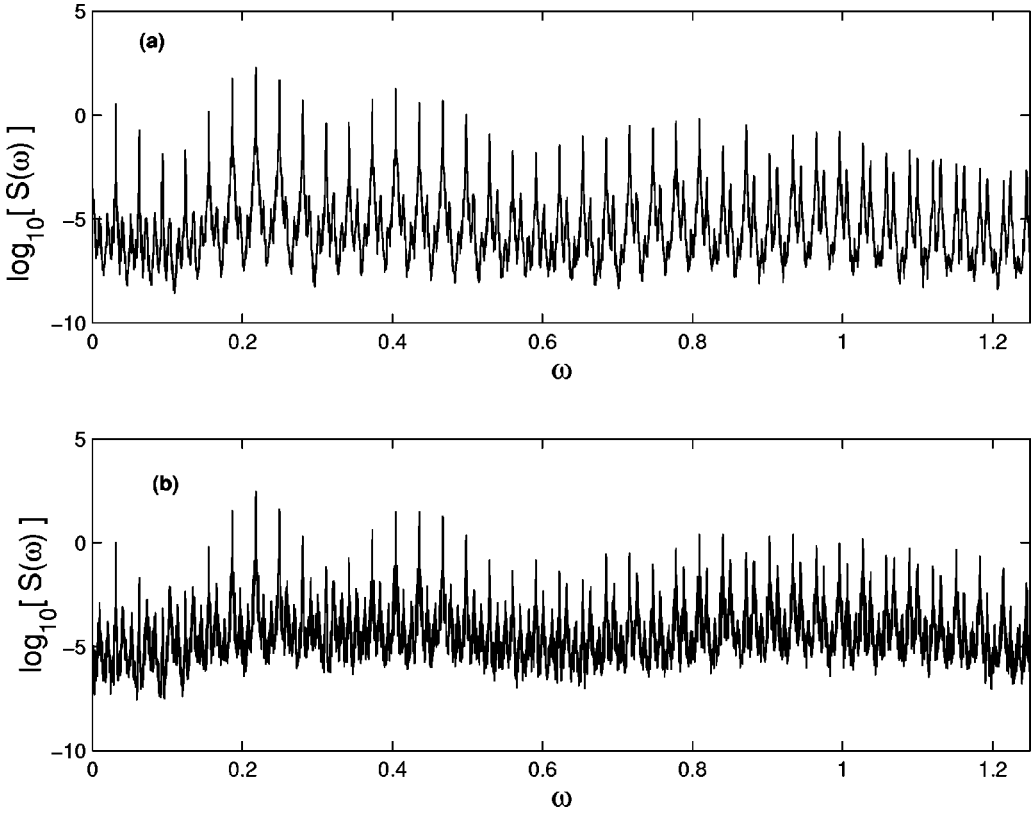

FIG. 6. The temporal power spectrum $S(\omega)$ of $u(\mathbf{x},t)$ for (a) data from the large-spiral region of MP and (b) for data from MN.

Before collecting data for averages, we allow transients to die out for $\tau_T \simeq 50\,000$ time units. (For comparison we note that the characteristic time scale for one spiral rotation is $\simeq 4-6$ time units.) We have checked in a few cases that our results are unchanged if we increase τ_T by a factor of 4. After these transients have died down and the statistical steady state has been obtained, we collect data for τ_{av} time units. For $C(t)$ and $P(\theta)$, we find that $\tau_{av} \simeq 50\,000$ suffices; for λ_m we find good convergence for $\tau_{av} \simeq 5000$ time units. For other quantities, like the defect density ρ with PBC, it is necessary to obtain data for 200 000 time units for the system sizes we use. The reason for this is the divergence in characteristic times near the S-M boundary with PBC, which leads to a very slow temporal variation of ρ with time.

TABLE I. The frequencies ω for the first eight most intense peaks in the temporal power spectrum of $u(\mathbf{x},t)$ in the states MP and MN. Data for the state MP are obtained from a point $\mathbf{x}$ that lies in the large-spiral region [Fig. 1(b)]. Both datasets were obtained at $\varepsilon = 0.0641$. In both these states these intense peaks can be indexed as $n_1\omega_1 + n_2\omega_2$, where n_1 and n_2 are integers and ω_1/ω_2 is irrational at the level of our numerical resolution. We obtain $\omega_1 \simeq 0.218\ldots$ and $\omega_2 \simeq 0.249\ldots$.

State MP			State MN		
ω	n_1	n_2	ω	n_1	n_2
0.218	1	0	0.218	1	0
0.249	0	1	0.249	0	1
0.0315	−1	1	0.187	2	−1
0.1865	2	−1	0.280	3	−1
0.2805	−1	2	0.373	2	0
0.4045	3	−1	0.405	1	1
0.4360	2	0	0.438	−4	5
0.4670	1	1	0.467	−1	2

III. NONEQUILIBRIUM STEADY STATES

We now turn to a detailed description of the properties of the nonequilibrium statistical steady states S, MP, MN, T1, and T2, the transitions, if any, between them, and their dependence on boundary conditions. We first consider the properties of the states S, MP, and MN and then the MP-S and MN-S transition. Next we describe the properties of the states T1 and T2 and then study the MP-T1 and MN-T1 transitions.

A. The S, MP, and MN states

As we will show below, the temporal behavior of S is simple [1,8]: the variables $u(\mathbf{x},t)$ and $v(\mathbf{x},t)$ are periodic in t. This arises because spirals rotate with a uniform frequency. However, the spatial organization of these spirals in S can be quite disordered. The precise organization depends on the initial condition we start with: If we start with a single large spiral and NBC the spiral core does not meander but the arms rotate rigidly at a fixed frequency; but if, say, we quench to S from T1 with PBC, we get a spatially disordered array of spirals whose number depends on the precise initial condition used. Our data for S below are obtained with PBC; we have checked in representative cases that the temporal correlation functions and distributions are qualitatively unchanged with NBC.

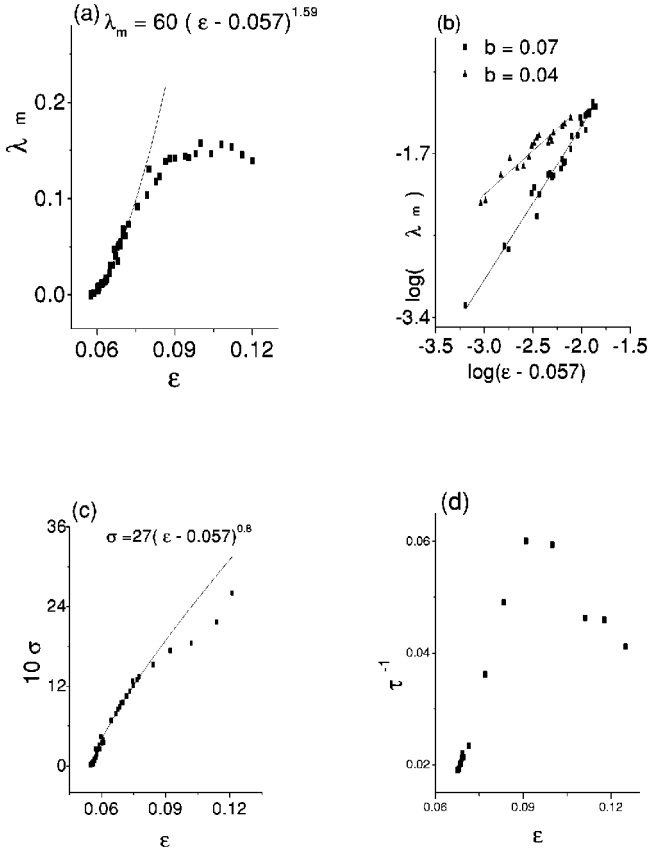

FIG. 7. The ε dependence of (a) λ_m at $b=0.07$; (b) λ_m at $b=0.04$ on a ln-ln (base 10) plot with the data of (a) superposed; (c) the width σ of $P(\theta)$; and (d) the inverse correlation time τ^{-1} from the decay of $C(t)$ vs ε. The lines indicate power-law fits in (a), (b), and (c); data in (a), (b), and (c) are averaged over three initial conditions.

In the state S the spiral tips rotate on circular trajectories. The rigidly rotating spiral waves in the system cause the local phase portraits to be strictly periodic with all the points condensing onto a single curve [Fig. 3(a)]. Consequently the temporal autocorrelation function of the fast variable $C(t) \equiv \langle u(\mathbf{x},t_0)u(\mathbf{x},t_0+t)\rangle$ is oscillatory and does not decay [Fig. 3(e)].

The time series of the fast variable $u(\mathbf{x},t)$ consist of trains of pulses [Fig. 5(a)]. These yield the distribution $P(\theta)$ of interspike intervals as described above. In the state S we find $P(\theta)\sim\delta(\theta-\theta_0)$, with $\theta_0\simeq 4.17$, which agrees with our estimate for the inverse angular frequency $\omega_0^{-1}\simeq 4.13$ that we get from the Fourier transform of $C(t)$ here [Fig. 3(e)]. The maximum Lyapunov exponent $\lambda_m<0$ in S ($\lambda_m=-0.04\pm 0.02$ for $\varepsilon=0.057$), i.e., this state is not chaotic. On increasing ε above $\varepsilon_c=0.057$ [15] the spirals start to meander, i.e., the tip of a single spiral no longer traces a circular path but an epicyclic one. This phenomenon has been observed in several models of excitable media [4,16].

The state MN consists of a single spiral. This is because the Neumann boundary condition acts as an absorbing boundary and all defects hitting the boundary are annihilated. Eventually, this leaves at most one spiral within the system. The temporal behavior of the state MN is quasiperiodic. This is borne out by the following observations: (1) The maximum Lyapunov exponent $\lambda_m\simeq 0$. (2) The temporal autocorrelation function $C(t)$ does not decay but oscillates. (3) The Fourier transform of $C(t)$; i.e., the power spectrum $S(\omega)=\langle 1/2\pi\int_{-\infty}^{\infty}dte^{i\omega t}u(\mathbf{x},t)|^2\rangle$, at a representative point $\mathbf{x}$, shows peaks at frequencies of the form $n_1\omega_1+n_2\omega_2$ with n_1 and n_2 integers and ω_1 and ω_2 irrational at the level of our numerical simulation. We identify ω_1 and ω_2 with the rota-

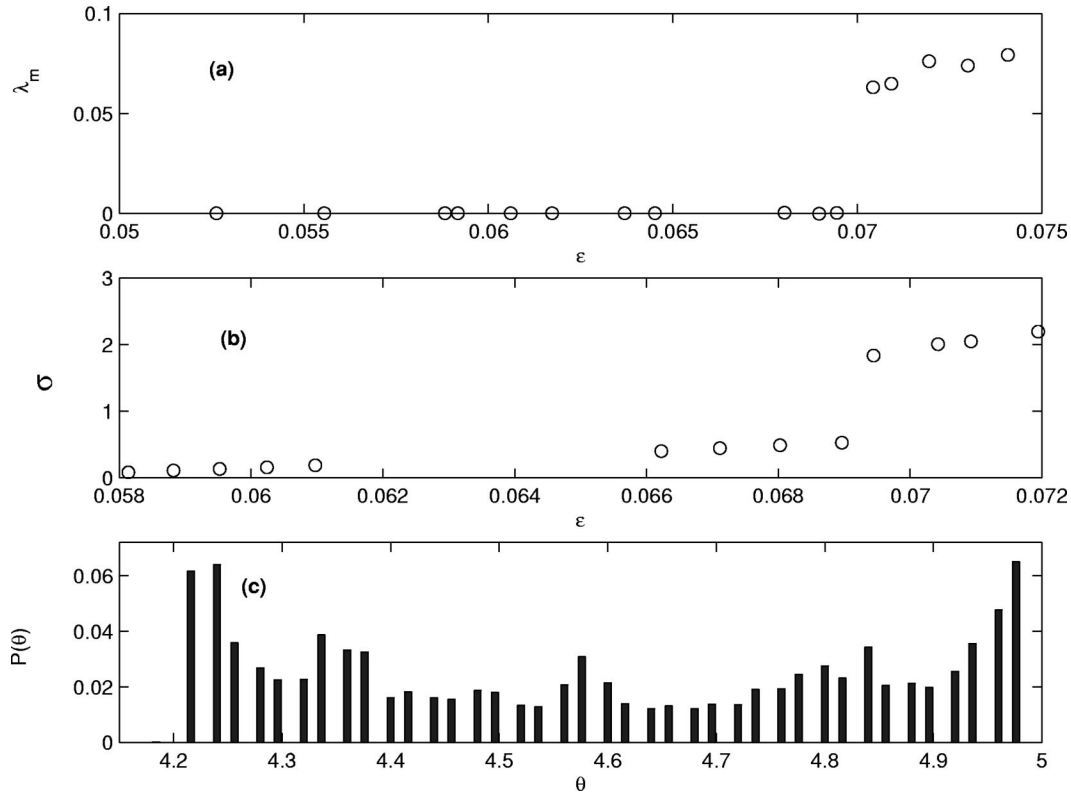

FIG. 8. Plots of (a) λ_m and (b) σ vs ε and (c) the distribution $P(\theta)$ for $\varepsilon=0.063$ for NBC. The linear system size $L=64$.

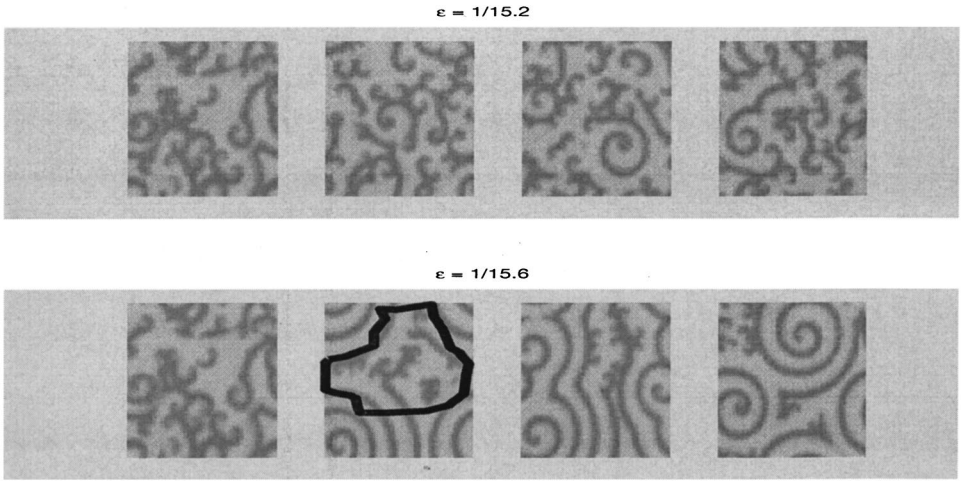

FIG. 9. Gray-scale plots of the u field at (a) $\varepsilon = 1/15.2 \simeq 0.0657$ and (b) $\varepsilon = 1/15.6 \simeq 0.0641$. The leftmost figures of each panel show the initial configurations just before the quench from T1 to MP. In each panel, the second, third, and fourth figures are separated by 50 000 time units from each other. The first and second figures in each panel are separated by 200 000 time units. In the second panel of (b) we indicate roughly by a solid line the interface between the state dominated by large spirals and the one dominated by pointlike defects.

tion and meander frequencies of the spiral, respectively, [Fig. 6(b) and Table I]. (4) The local phase portrait shows that a band gets filled densely. (5) Finally the distribution $P(\theta)$ is bimodal [Fig. 8(c)].

The state MP is inhomogeneous, consisting of large spirals coexisting with pointlike defects [Fig. 1(a)]. This state possesses a small but positive λ_m. Given the inhomogeneous nature of the state MP, the local phase portraits change qualitatively with spatial location $\mathbf{x}$. If they are calculated in a region dominated by a large spiral, they display a structure similar to that in MN [Fig. 4(a)]; however, if they are calculated in a region dominated by pointlike defects, they display a noisy structure. In MP, the globally averaged temporal autocorrelation function $C(t) \sim \exp(-ct^{\gamma})\cos(\omega t + \delta)$ with $\gamma < 1$. However, due to the inhomogeneous nature of state MP, this naive global average should not be performed. If $C(t)$ is calculated with time series from a region dominated by large spirals, it scarcely decays on the time scales of our simulations [Fig. 4(c)]. Its Fourier transform, i.e., the power spectrum of this time series, has a peak structure similar to that in state MN [see Fig. 6(a) and Table I]. If $C(t)$ is calculated with time series from a region containing pointlike defects, its envelope decays more rapidly [Fig. 4(d)]; however, the decay is still too slow to allow us to fit it convincingly here.

In state MP, the probability distribution $P(\theta)$ depends on the spatial location $\mathbf{x}$: If we calculate $P(\theta)$ in a region containing a large spiral, we find that it is bimodal; however, if we calculate $P(\theta)$ in a region dominated by pointlike defects, we find that it is broad [Figs. 4(e), 4(f)]. The qualitative shape of $P(\theta)$ in a region dominated by pointlike defects differs from that calculated in T1: It displays a sequence of peaks with an exponentially decaying envelope. Similar multimodal probability distributions with exponentially decaying envelopes are seen in periodically stimulated excitable media [17]. We believe the large spiral provides such periodic (or quasiperiodic) stimulation to the pointlike defect region leading to the multimodal PDF of Fig. 4(f).

As noted above state MP displays coexistence of large spirals and pointlike defects: It has been mentioned briefly in Ref. [1] that a sudden change of ε, which takes the system from T1 to MP, results in a binary mixture of spirals and point defects; and the relaxation behavior has been likened to that of a ''binary glass.'' We explore this point of view in detail below.

In equilibrium statistical mechanics the analogs of nonequilibrium statistical steady states like S, MP, MN, T1, and T2 are the equilibrium phases of a system. As parameters such as the temperature are changed, these phases can undergo transitions, the most common being a first-order phase transition at which thermodynamic functions jump discontinuously. The MN-T1 transition is the nonequilibrium analog of such a transition. If the phase diagram is depicted in a p-dimensional parameter space of ''field-type'' variables, such as the chemical potential, temperature, or magnetic field, then first-order phase boundaries are $(p-1)$-dimensional hypersurfaces along which two equilibrium phases coexist. If, instead, the phase diagram is depicted using one or more ''density-type'' variables, such as the density of a liquid or the magnetization density, then the region of phase coexistence can be p dimensional. A simple example is furnished by the Ising ferromagnet in spatial dimensions $d > 1$: In the magnetic field H and temperature T plane, the first-order phase boundary is the line $H = 0$, $0 \leqslant T < T_c$, where T_c is the Curie temperature; in the T-M plane, where M is the magnetization, this first-order boundary is replaced by a two-dimensional region of two-phase coexistence that lies below the coexistence curve [18].

If we pursue this analogy with equilibrium phase diagrams, then b and ε seem to be field-type variables (like the temperature and magnetic field), so we should expect first-order boundaries to be lines in the b-ε plane (since we work at a fixed value of b, we should intersect these lines at points as we vary ε). Indeed, the first-order MN-T1 transition with NBC satisfies this expectation. It is peculiar, therefore, that, with PBC, the state MP appears to be a binary mixture (a region of two-phase coexistence in our equilibrium analogy) over a finite extent of the ε line. However, such phase coexistence over a finite extent of parameter space is not unknown in nonequilibrium systems. The example that has been studied most clearly from this perspective is the probabilistic cellular automaton known as the Toom-NEC model [19]. We now present some data to elucidate this view of the state MP. Figures 9(a), 9(b) show gray-scale plots of the u field at times separated by intervals of 50 000 time units (approximately 12 500 spiral rotations) following a quench from T1 to MP. The spontaneous nucleation of spirals from an initial condition consisting entirely of point defects can be seen. These large spirals do not grow beyond a point, but

simply drift. Visual observations of successive configurations show that these spirals are destroyed by collision with pointlike defects and other large spirals, and spontaneously nucleate when a given pointlike vortex is isolated from its neighbors for a sufficiently long time. The entire system is observed to be in a dynamic statistical steady state.

This evolution should be viewed as the coarsening of a two-state (or two-phase) mixture in which one of the states is dominated by one or a few macroscopic spirals and the other state comprises a collection of small pointlike defects. As in the growth of domains of two coexisting phases (after a quench from a one-phase regime to a two-phase region), the sizes of islands of a given state grow in time [20] up to a crossover time fixed by the system size. Small systems completely phase separate into regions with large spirals and point defects within the time scale of our simulations. Systems with larger sizes take longer to reach a completely phase-separated state and it is difficult to reach it for $L>64$ in our simulations. A completely phase-separated state can be seen clearly in Fig. 9(b), where ε is not too close to the MP-T1 boundary. Visual observation of the states over the time interval covered by the panels in Fig. 9(b) show the following: (1) The interface between the large-spiral state and the point-defect state fluctuates; (2) occasionally the large spiral becomes two or three times smaller, but still macroscopically large, spirals; (3) in the point-defect region the cores move in an irregular fashion [see, e.g., Fig. 1(b)]. Not surprisingly, as ε approaches the MP-T1 boundary, from the MP side [Fig. 9(a)], fluctuations increase, reduce the sizes of large spirals, and so the distinction between the large-spiral state and the point-defect state becomes less clear. Note that the first figure in each panel in Figs. 9(a), 9(b) shows the initial states used in both cases; clearly, relative to these initial states, the subsequent patterns in Fig. 9(a) and 9(b) have coarsened. The clear phase separation visible in Fig. 9(b) becomes less clear in Fig. 9(a), which is obtained with parameters nearer the MP-T1 boundary, where we expect more fluctuations. These fluctuations, evident from even a cursory comparision of successive panels in Fig. 9(a), are analogous to those in, say, the two-dimensional Ising model in the two-phase region slightly below the critical temperature T_c. Proximity to T_c results in large fluctuations and contorted interfaces that are often hard to pinpoint configuration by configuration; also, there can be droplets of many sizes, each with an interface separating it from a region of the other coexisting phase; these interfaces form and break dynamically. In Sec. III D below we introduce an order parameter that helps us to find the MP-T1 boundary.

As discussed above, all the observables that we have measured indicate that the large spirals in MP meander while the point defects execute irregular motion. Since $\lambda_m>0$ in MP, but not in MN, we conjecture that the chaos in this state arises because of the motion of the pointlike defects.

It is instructive to contrast the state MP with PBC with a similar state obtained in oscillatory media just below the transition to spiral breakup. In such media it has been conjectured [21] that the convective instability of travelling waves in this system causes the growth of large spirals on quenching the system below the defect–chaos-transition boundary. These large spirals eventually dominate the system at long times resulting in glassy states. It has been argued [22] that there is no convective instability of waves in Eq. (1), but instead a direct transition to an absolute instability at their M-T1 transition boundary [23]. Thus, the MN-T1 boundary at $\varepsilon\simeq 0.0699$ follows the stability line of a single large spiral. Since the large spirals in MP coexist with pointlike defects, one might think that interactions between them should change the transition point obtained from the single-spiral stability analysis. We find, however, that the MP-T1 transition boundary is almost unchanged $\varepsilon\simeq 0.0689$. Thus we conjecture that this line also marks the stability limit of large spirals embedded in a sea of pointlike defects as in MP. Below this line, in MP, nucleated large spirals will not grow because of the absence of a convective instability in the system. We feel that this accounts for the coexistence of large spirals and point defects in MP. In MN, drifting point defects hit the system boundary and annihilate with their virtual mirror images, leading to a decay of the vortex number with time, till only a single large spiral remains in the system.

B. The S-MP and S-MN transitions

Spirals in excitable media display a phenomenon termed meander: In a certain region of the stability diagram, the spiral tips no longer move on circular trajectories but on epicyclic ones. Model (1) displays a second meandering regime (the states MP or MN) at higher values of ε compared to the standard FitzHugh-Nagumo model.

We observe a continuous transition from S to MP. At the S-MP transition in model (1) we find that as ε increases across the S-MP boundary, the time series for $u(\mathbf{x},t)$ becomes irregular, and the globally averaged $P(\theta)$ broadens. Its width scales as $\sigma\sim(\varepsilon-\varepsilon_{c\sigma})^{\Delta_\sigma}$, with $\varepsilon_{c\sigma}=0.057\pm 0.002$, $\Delta_\sigma=0.80\pm 0.02$, and $\varepsilon\downarrow\varepsilon_{c\sigma}$. We find that the state MP is *chaotic*. The maximum Lyapunov exponent decreases smoothly to zero as $\varepsilon\downarrow\varepsilon_c$. At the S-MP transition, we observe that $\lambda_m\sim(\varepsilon-\varepsilon_{c\lambda})^{\Delta_\lambda}$ for $\varepsilon\downarrow\varepsilon_{c\lambda}$ [Fig. 7(a)], with $\varepsilon_{c\lambda}=0.056\pm 0.002$ for $b=0.07$ (note that $\varepsilon_{c\lambda}=\varepsilon_{c\sigma}\equiv\varepsilon_c$) and $\varepsilon_{c\lambda}=0.057\pm 0.001$ for $b=0.04$. Given the resolution of our calculation [24] the exponents Δ_λ seems nonuniversal: $\Delta_\lambda=1.59\pm 0.2$ for $b=0.07$ and $\Delta_\lambda=0.8\pm 0.1$ for $b=0.04$ [Fig. 7(b)]. We note that $\Delta_\sigma\sim 2\Delta_\lambda$ thus implying that near the S-MP boundary, $\sigma\sim\sqrt{\lambda_{max}}$. We have already noted that the state MP is inhomogeneous. The vortex cores in the point-defect regions drift at a slower rate as the S-MP transition is approached, eventually freezing in the state S. The large spiral meanders and we conjecture that it behaves like one in MN.

We have already noted that the state MP is inhomogeneous. The vortex cores in the point-defect regions drift at a slower rate as the S-MP transition is approached, eventually freezing in the state S. The large spirals meander and we conjecture that they undergo a transition similar to the S-MN transition. If we quench the system from T1 to ε values near the S-MP boundary, many small spirals are seen to nucleate whereas, in a similar quench near the MP-T1 boundary, only a few spirals are seen [1]. This may be explained by assuming that a pointlike defect grows a spiral arm if it becomes isolated from its neighbors by more than a certain distance R. Assuming that point defects move with a mean velocity V and a point defect needs a time Δt to form a spiral arm, then the typical radius needed to nucleate a spiral will be $V\Delta t$.

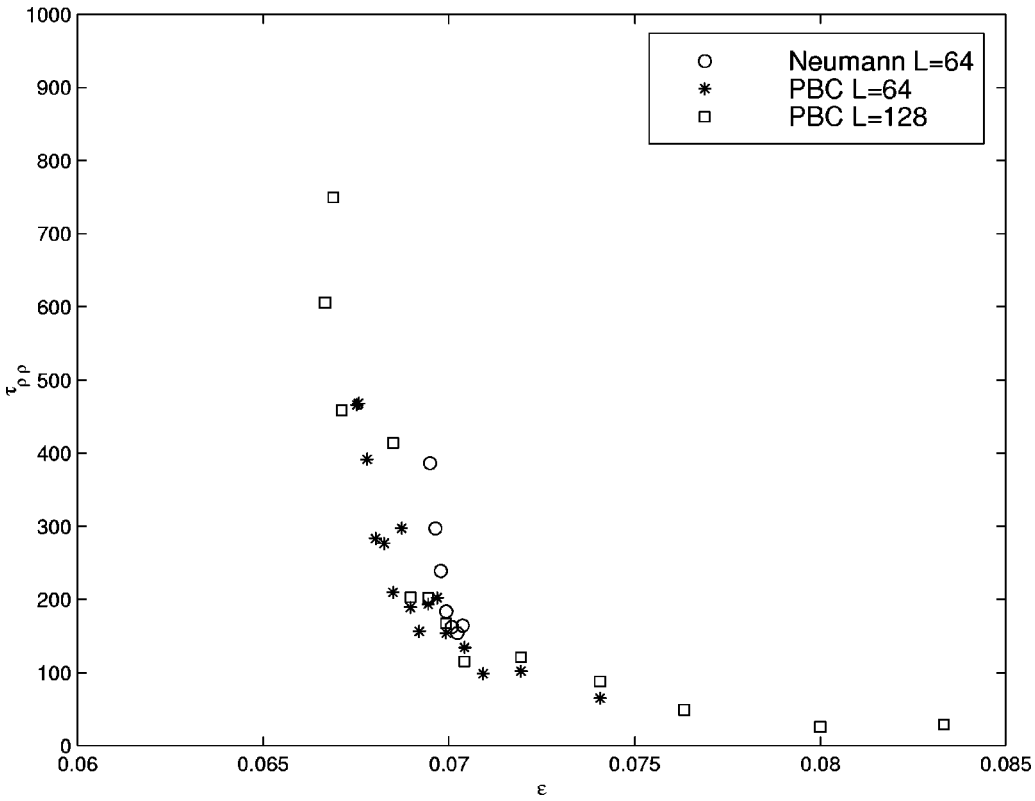

FIG. 10. The decay time $\tau_{\rho\rho}$ of $C_{\rho\rho}(t)$ as a function of ε near the MP-T1 boundary. Data for $L=128$ and $L=64$ with PBC and $L=64$ with NBC are plotted.

Since the mean velocity of the point defects goes to zero at the S-MP boundary, the radius needed to nucleate a spiral in a sea of point defects should also shrink. Note that these small spirals near the S-MP boundary arise because of improper annealing, since they are prevented from aggregating on observable time scales due to the slowing down of all motion here. We expect that at very long times they will aggregate into large spirals, and the true asymptotic state will be a phase-separated one.

With Neumann boundary conditions, the asymptotic state is a single spiral that meanders in MN and moves on a simple closed trajectory in S; in this MN state $\lambda_m \simeq 0$ and the disribution $P(\theta)$ is bimodal because of the quasiperiodicity elucidated above (Table I). Since quantities like $\lambda_m \simeq 0$ in MN, it is difficult to decide numerically whether the S-MN transition is continuous or not. We conjecture that it is, since work on the standard FitzHugh-Nagumo equation [4] [model (1) with $f(u)$ replaced by u] has shown that the transition of a single spiral to meander is a Hopf bifurcation in a frame of reference rotating with the spiral core. This has also been seen in free-boundary models of excitable media and is expected to be a generic phenomenon [16].

Since $\lambda_m \simeq 0$ in MN but $\lambda_m > 0$ in MP, we conjecture that it is the motion of the pointlike defects that is responsible for the chaotic nature of MP. We also conjecture that the gradual freezing of the motion of these defects at the S-MP transition is responsible for the continuous nature of the S-MP transition.

C. States T1 and T2

The state T1 is characterized by the steady creation and annihilation of spiral defects. In the local phase portrait of Fig. 3(i), the points spread out further than in Fig. 3(e), but remain more-or-less bounded in the region enclosed by the closed loop in Fig. 3(a). This spreading out is even more pronounced in the state T2 [Fig. 2(d)]. In the states T1 and T2, the envelope of $C(t)$ decays as $\exp(-t/\tau)$ but the decoherence increases (i.e., τ falls) as we move from to T1 to T2 [Fig. 7(d)]. The plot of σ vs ε flattens out as we move from T1 to T2. We do not see any sign of nonanalytic behavior at the T1-T2 transition in plots of λ_m vs ε. The work of [6] indicates that the states T1 and T2 are spatiotemporally chaotic and possess similar Lyapunov dimension densities in the thermodynamic limit irrespective of the boundary conditions. In both T1 and T2, the results for the quantities we measure are not affected qualitatively if we go from PBC to NBC; however, the precise numerical values are changed (e.g., $\lambda_m \simeq 0.079$ at $\varepsilon \simeq 0.074$ with NBC and $\lambda_m \simeq 0.107$ at the same point with PBC). In the states T1 and T2, the temporal autcorrelation function of the defect number $C_{\rho\rho}(t)$ decays as $C_{\rho\rho}(t) \sim \exp(-t/\tau_{\rho\rho})$. We find that $\tau_{\rho\rho}$ becomes very large in MP as we move away from the MP-T1 boundary. We conjecture that this is due to the slowing down of motions as the S-MP transition is approached (see Fig. 10); $\tau_{\rho\rho}$ becomes so large in MP that we cannot compute it reliably deep in this state in our numerical studies.

D. The MN-T1 and MP-T1 transitions

The breakdown of a single well-formed spiral occurs as we move from MN to T1. It can be empirically explained as follows [1]: In T1 the Doppler effect caused by the meandering of the spiral core causes the propagation velocity of some

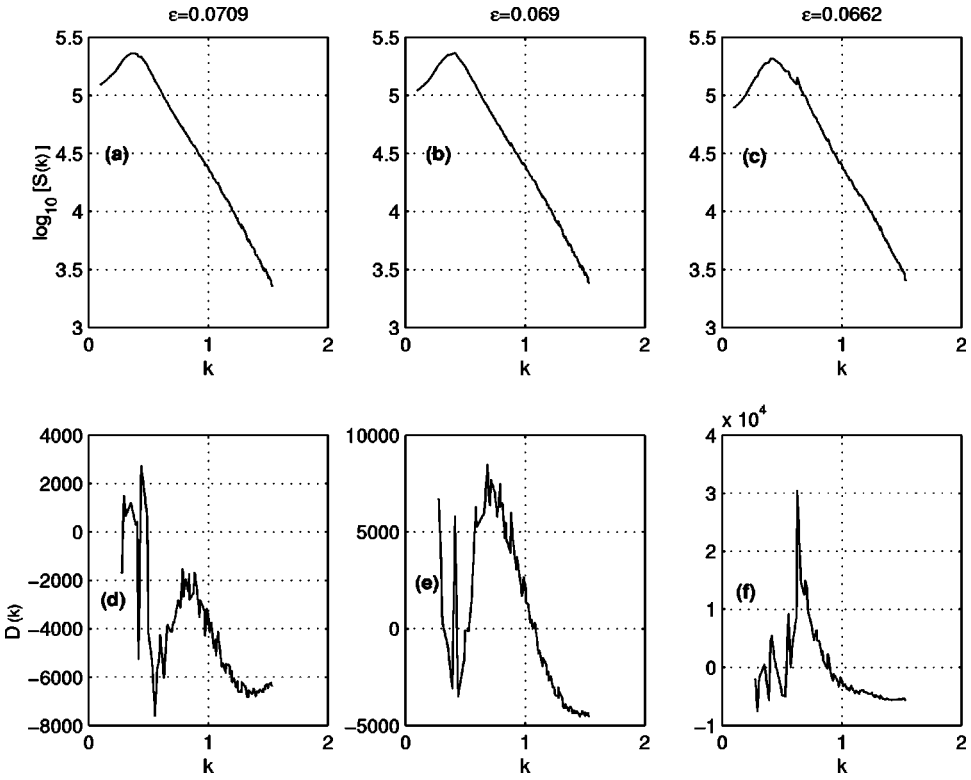

FIG. 11. The spatial power spectrum $S(k)$ (see text) vs k for values of ε in (a) T1, (b) near the MP-T1 boundary in MP, and (c) deep in MP. (d)–(f) The data of (a)–(c) with the Lorentzian background (see text) subtracted off [denoted by $D(k)$] to display the formation of the secondary peak in $S(k)$, which signals the formation of MP.

region of the arm to fall below the minimum speed of a plane wave in the medium. Since the spiral arm is nearly a plane wave far from the spiral core, that region of the spiral arm cannot propagate and is destroyed, resulting in the formation of a broken-wave segment. Each of these pieces in turn curl up into spirals and the process of breakdown repeats. Finally a statistical steady state is reached in which there is dynamic creation and annihilation of defects.

The MN-T1 transition is discontinuous. With typical initial conditions in MN one spiral starts growing and eventually drives all the other spirals out of the system. We have checked this by doubling the system size. On crossing the MN-T1 boundary, this single spiral disintergrates into many spirals, leading to discontinuities in the variations of ρ [Fig. 2(a)], λ_m, and σ [Figs. 8(a), 8(b)] with ε. We observe hysteresis in ρ on crossing from MN to T1 by changing ε at a finite rate [Fig. 2(b)].

As we have stated earlier, the state MP is inhomogeneous, consisting of large spirals coexisting with pointlike defects. Thus we may identify the MP-T1 transition by visually not-

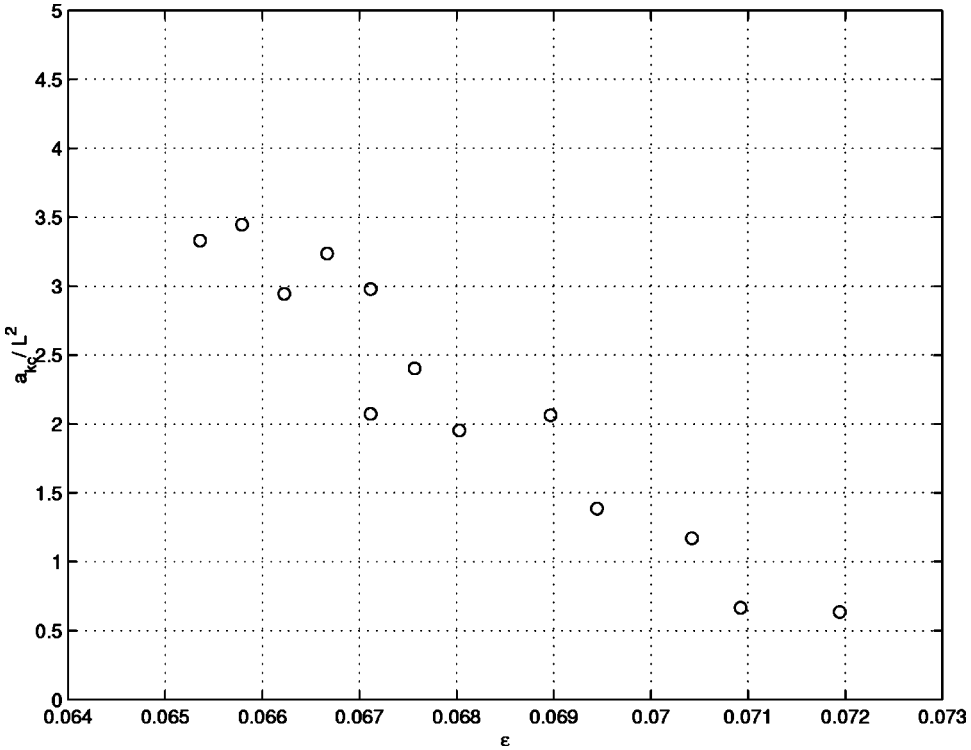

FIG. 12. The amplitude a_{kc} of the secondary peak of $S(k)$ (see text) as a function of ε. The amplitude is normalized by L^2 with $L=64$.

ing the locus in the parameter space where such an inhomogeneous mixture ceases to exist. Since the time-scale for which large spirals survive is visually observed to go to zero as the MP-T1 boundary is approached from the MP side, this method does not give the exact boundary; we obtain $\varepsilon_{vis} \simeq 0.0689$. It is useful, therefore, to define an order parameter, as is done in statistical mechanics, to characterize the presence of large spirals. The presence of the periodic spiral arms gives a sharp peak in the structure factor of the u field in MP. Figure 11 shows, respectively, plots of the circularly averaged spatial power spectrum $S(k) = 1/2\pi \int d\theta S(k\cos(\theta), k\sin(\theta))$ vs k. A secondary peak shows up in MP [Fig. 11(a)]; its size decreases as we near the MP-T1 transition boundary [Fig. 11(b)] and it is not present in T1 [Fig. 11(a)]. This peak shows up more clearly if we subtract off the background (which we fit to a Lorentzian since the spatial correlation function of $u(\mathbf{x},t)$ decays as an oscillatory exponential); these peaks are shown in Figs. 11(d)–11(f). Our visual observations show that in MP, as L increases, more and more large spirals nucleate. It is natural, therefore, to assume that there is a finite density of large spirals. As a result, the peak in the structure factor should also increase with the system size giving a true order parameter in the thermodynamic limit $L \to \infty$. A plot of a_{kc}, the peak height normalized by L^2, is shown as a function of ε in Fig. 12. The order parameter plotted in Fig. 12 goes from $\simeq 3.5$ to $\simeq 0.5$. We have tried to obtain a_{kc} from the secondary peak that clearly develops in Fig. 11 as we go from T1 to MP. This entails fitting the background peak in $S(k)$, subtracting it from our data, and then numerically integrating the remainder to estimate a_{kc}. This procedure is quite noisy, principally because of the subtraction of the fitted background peak. We have tried the forms $S(k) = [(k-k_0)^2 + \beta^2]^{-1}$ and $S(k) = \int_0^{2\pi} d\theta [k^2 + k_0^2 - 2kk_0\cos(\theta) + \beta^2]^{-1}$ for the background peak in Fig. 11 (the data shown in Fig. 12 are obtained with a background peak parametrized as $S(k) = [(k-k_0)^2 + \beta^2]^{-1}$). Both forms give reasonable fits, but $a_{kc} \simeq 0.5$ is essentially our noise level, e.g., we have tried to use our fitting procedure in T1, where the secondary peak of Fig. 11 is clearly absent; and there too we find $a_{kc} \simeq 0.5$. Thus we believe that the data of Fig. 12 are consistent with a_{kc} vanishing at the MP-T1 boundary; of course, conclusive proof for this can only be obtained by studies of much larger systems than are possible with our computational resources. Note that Fig. 12 is consistent with an MP-T1 boundary of $\varepsilon \simeq 0.0699$, which agrees with our visually observed MP-T1 boundary of $\varepsilon_{vis} \simeq 0.0689$.

IV. CONCLUSIONS

We have carried out the most extensive numerical study of model (1) especially with a view to elucidating the nature of its statistical steady states and transitions between them. Our work is guided by studies of phase diagrams and phase transtions in equilibrium statistical mechanics. Since nonequilibrium systems like model (1) do not have any free energy, we define transitions between its statistical steady states as the loci of points in parameter space at which one or more densities or correlation functions show nonanalytic behavior. Unlike the bulk phase diagrams of equilibrium systems, the stability diagram of model (1) shows a sensitive dependence on boundary conditions and initial conditions. This is not unknown in systems with nonequilibrium steady states [25]; however, to the best of our knowledge, such boundary-condition dependence of stability diagrams has not been studied systematically for any set of deterministic partial differential equations that exhibit spatiotemporal chaos. Our detailed study is a first step in this direction. Our study reveals that the state with meandering spirals depends most sensitively on the boundary conditions: With NBC we get MN, which has one large quasiperiodically rotating spiral. If, instead, we use PBC, MP obtains with large, quasiperiodically rotating spirals coexisting with small pointlike defects that move irregularly. (As we have explained above, such coexistence is quite remarkable.) It is not surprising, then, that the MP-T1 and MN-T1 transitions are qualitatively different: The former is continuous and is characterized by the order parameter a_{kc}, which we have defined above; the latter is discontinuous or first-order with a jump in the defect density ρ or the maximun Lyapunov exponent λ_m at the transition. Nevertheless, both MP-T1 and MN-T1 lie quite close to each other and also to the point at which the field configuration of a single spiral becomes linearly unstable [22]. We conjecture that this instability precipitates both MP-T1 and MN-T1 transitions; however, the natures of these transitions are dictated by the properties of MP and MN, which in turn depend sensitively on the boundary conditions. Thus, though the linear instabilities of reference states may determine the rough stability diagram of the system [26], the boundary conditions are equally important.

The MP-S and MP-N transitions are also qualitatively different. At the former the irregular motion of the small, pointlike defects becomes slower and slower and the meander frequency of the large spirals tends to zero. At the MN-S transition there are no small pointlike defects; all that happens here is that the single large spiral stops meandering. It is natural to conjecture, therefore, that the MN-S boundary is precisely the locus of points at which a Hopf bifurcation (in a frame rotating with the spiral arm) signals the onset of the meander transition.

Our study has direct implications for the CO oxidation experiments on Pt(110) [1]: The parameter ε is related to the ratio of two rate constants that depend on the temperature T in an Arrhenius fashion. Thus, by changing T one can change ε and study the transitions elucidated in our study. In addition to suggesting such quantitative tests, our study shows that local phase portraits, temporal autocorrelation functions, and the distribution $P(\theta)$ should provide effective ways of characterizing the CO oxidation reaction on Pt(110). It would be interesting to see if experiments could be performed with boundary conditions that yield a regime like MP.

ACKNOWLEDGMENTS

We thank A. Basu, B. Chakraborty, C. Dasgupta, H.R. Krishnamurthy, G.V. Pai, and S. Ramaswamy for discussions, CSIR (India) for support, and SERC (IISc, Bangalore) for computational resources.

[1] M. Bär and M. Eiswirth, Phys. Rev. E **48**, R1635 (1993); M. Hildebrand, M. Bär, and M. Eiswirth, Phys. Rev. Lett. **75**, 1503 (1995); M. Bär, M. Hildebrand, M. Eiswirth, M. Falcke, H. Engel, and M. Neufeld, Chaos **4**, 499 (1994).

[2] J. D. Lechleiter *et al.*, Science **252**, 123 (1993).

[3] A. T. Winfree, Science **266**, 1003 (1994); L. Glass, Phys. Today **49**, 40 (1996).

[4] D. Barkley, Phys. Rev. Lett. **68**, 2090 (1992).

[5] D. Barkley, Physica D **49**, 61 (1991); M. Doule *et al.*, Int. J. Bifurcation Chaos Appl. Sci. Eng. **7**, 11 (1997).

[6] M. C. Strain and H. Greenside, Phys. Rev. Lett. **40**, 2306 (1998).

[7] M. Bär, N. Gottschalk, M. Eiswirth, and G. Ertl, J. Chem. Phys. **100**, 1202 (1994).

[8] A. Pande and R. Pandit, in *Structure and Dynamics of Materials in the Mesoscopic Domain*, edited by B. D. Kulkarni and Moti Lal (Imperial College Press-The Royal Society, London, 1999).

[9] This is analogous to using the Fourier components ρ_G of the density $\rho(r)$ as the order parameters for the transition from a liquid to a crystalline solid. Visual observations show that on larger system sizes, there is a density of large spirals. Thus we conjecture that the peak in the structure factor will scale with system size giving a valid order parameter in the thermodynamic limit.

[10] For a given system size L, there is a time t_L after which large spiral patches aggregate. This time diverges with system size since large spiral patches nucleate at random on the grid and have to ''find'' each other. After this time, for a time t_L', observations obtained at any point in the large-spiral region will see quasiperiodic behavior and those from the pointlike defect region will see irregular behavior; t_L' is the mean time over which the large spiral region drifts across any observation point. This time will diverge with system size. Thus, while averaging data for the inhomogeneous state MP, averaging times should be $\lesssim t_L'$.

[11] T. Parker and L. Chua, *Practical Numerical Algorithms for Chaotic Systems* (Springer, Berlin, 1989), pp. 73–81.

[12] S. Chialine, M. Hasler, and A. Premoli, Int. J. Bifurcation Chaos Appl. Sci. Eng. **4**, 127 (1994).

[13] A. Pande, C. Jayaprakash, and R. Pandit (unpublished).

[14] W. H. Press *et al.*, *Numerical Recipies in C* (Cambridge University, London, 1995), pp. 714–722.

[15] It is possible that ε_c with PBC is different from ε_c with NBC, i.e., the S-MP and S-MN boundaries are different; however, given our numerical resolution, we cannot distinguish the two. Our value is consistent with that in Ref. [1].

[16] V. Hakim and A. Karma, e-print cond-mat/9903262.

[17] D. T. Kaplan, J. R. Clay, T. Manning, L. Glass, M. R. Guevara, and A. Shrier, Phys. Rev. Lett. **76**, 4074 (1996).

[18] P. M. Chaikin and T.C. Lubensky, *Principles of Condensed Matter Physics* (Cambridge University Press, Cambridge, 1998).

[19] C. H. Bennett and G. Grinstein, Phys. Rev. Lett. **55**, 657 (1985).

[20] In many equilibrium two-phase regimes the sizes of such domains grow as a power of time in the wake of a quench; however, slower growth laws, especially in disordered systems, are not unknown.

[21] G. Huber, P. Alstrøm, and T. Bohr, Phys. Rev. Lett. **69**, 2380 (1992).

[22] M. Bär and M. Or-Guil, Phys. Rev. Lett. **82**, 1160 (1999).

[23] It is not quite clear whether PBC's or NBC's have been used to determine the stability diagram of Ref. [1]. Some quantities (e.g., the spatial autocorrelation function of the defect density) are computed with PBC and others (e.g., the M-T1 boundary) are computed with NBC. Reference [1] also does not make the MP-MN distinction, which we elucidate here.

[24] We fit our data for each initial condition and use the standard deviation of the fitted parameters as the error.

[25] B. Schmittmann and R. K. P. Zia, in *Phase Transitions and Critical Phenomena*, edited by C. Domb and J. L. Lebowitz (Academic Press, New York, 1995), Vol. 17.

[26] M. C. Cross and P. C. Hohenberg, Rev. Mod. Phys. **65**, 851 (1993).